

Residual and tidal circulation revealed by VHF radar surface current measurements in the southern Channel Isles region (English Channel)

Alexei Sentchev^{a,*}, Philippe Forget^b, Yves Barbin^b

^aLaboratoire d'Océanologie et de Géosciences (CNRS-UMR8187), Université du Littoral - Côte d'Opale, 32 Av. Foche, 62930 Wimereux, France

^bLaboratoire de Sondages Electromagnetiques de l'Environnement Terrestre (CNRS-UMR6017), Université du Sud Toulon Var, 83130 La Garde, France

ARTICLE INFO

Article history:

Received 12 July 2008

Accepted 4 December 2008

Available online 13 December 2008

Keywords:

tidal current

residual current

VHF radar

Channel Isles region

ABSTRACT

Two very high-frequency radars (VHFRs), operating in the southern Channel Isles region (English Channel) in February–March 2003, provided a continuous 27-day long dataset of surface currents at 2 km resolution over an area extending approximately 20 km offshore. The tidal range in the region of study is one of the highest in the world and the coastal circulation is completely dominated by tides. The radar data resolve two modes which account for 97% of the variability of the surface current velocities, with the major contribution of the first mode. This mode accounts for oscillating tidal currents whereas the second mode represents motions emerging from the interaction of tidal currents with capes and islands (eddy in the vicinity of the Point of Grouin and jet south of Chausey). A fortnightly modulation of the modal amplitudes causes the exceptional (more than 600%) variability of currents which is well captured by the VHFR observations. The radar data revealed that tidal circulation in the region is flood-dominated with a strong asymmetry of current velocity curve. Wind events and fortnightly variability affect the course of tidal cycle by modifying the magnitude and duration of ebb and flood. In addition to expected features of coastal circulation (tidally dominated flow, eddies) and high wind-current coupling, the residual currents revealed a strong cross-shore structure in the mean and a significant variability which has the same order of magnitude.

© 2008 Elsevier Ltd. All rights reserved.

1. Introduction

In recent years, high-frequency (HF) Doppler radar systems have had stunning success in the mapping of surface currents. The ability to map surface circulation in coastal ocean areas has brought new insights to the complexities of physical processes in nearshore waters, and allowed significant advances in our understanding of circulation and oceanographic conditions in many coastal regions (e.g. Prandle, 1993; Shay et al., 1998; Marmorino et al., 1999; Haus et al., 2000; Breivik and Sætra, 2001; Kovacevic et al., 2004; Bassin et al., 2005; Kaplan et al., 2005; Kosro, 2005; Yoshikawa et al., 2007).

Very high-frequency radar (VHFR) system operated in the English Channel in spring 2003 on two different sites (southern part of the Channel Isles region and along the Opal coast in the Dover Strait), and has provided high resolution surface current maps which shed a light on small scale features and extreme variability of coastal water dynamics.

The circulation in the English Channel has been studied previously by many authors by means of numerical modeling (Pingree and Maddock, 1985a; Orbi and Salomon, 1988; Bailly du Bois and Dumas, 2005; Sentchev et al., 2006), remote sensing (Ménésien and Gohin, 2006), field measurements (Lafite et al., 2000), and also radar observations of the currents. The earliest radar measurements of surface circulation in the English Channel have been performed at the beginning of eighties. Broche et al. (1987) reported the results of 3-day long VHFR measurements in the Bay of Seine. In 1990–1991, Prandle et al. (1993) conducted an intense nearly year-long HFR experiment in the Strait of Dover, which allowed to obtain relatively accurate estimates of the tidal flow into the North Sea. The water dynamics in the French sector of the Strait of Dover derived from radar measurements has been recently described by Sentchev and Yaremchuk (2007). It was shown that a discontinuity in current velocity field, observed approximately 10 km offshore, is caused by the reversal in the sign of rotation of surface current vectors due to bottom friction and stratification effects. This provides surface current convergence on ebb and divergence on flood. The line of convergence approximately follows the 30-m isobath.

In the present study we focus on physical processes governing the tidal and residual circulation in the southern Channel Isles

* Corresponding author.

E-mail addresses: alexei.sentchev@univ-littoral.fr (A. Sentchev), philippe.forget@lseet.univ-tln.fr (P. Forget), yves.barbin@lseet.univ-tln.fr (Y. Barbin).

region which will be referred hereafter as SCIR (Fig. 1). A unique combination of historical heritage, tourism, aquatic industry, makes this region of considerable commercial and ecological interest, and requires new concepts of ecologically sustainable development. Nevertheless, recent experimental or modeling studies of the marine environment in SCIR, are rather scanty. With the exception of earlier modeling studies of tidal and residual circulation in the SCIR performed by Pingree and Maddock (1985a), Orbi and Salomon (1988) and Le Hir et al. (1986), authors did not find any results relevant to a detailed description of the SCIR dynamics in literature. Small scale features of circulation, their magnitude and dependence on various forcing factors remain relatively uncertain. This shortcoming is primarily due to the difficulties in acquisition of long-term *in situ* data because of the extremely strong currents and

severe meteorological conditions in this part of the Channel. In that respect, remote sensing of surface currents by VHF radars provides a unique opportunity to establish a monitoring system in the SCIR on a regular basis.

The first step in the description of fine scale circulation patterns derived from VHFR measurements in the eastern English Channel (EEC) has been done by Sentchev and Yaremchuk (2007). The present work can be considered as an extension of the above mentioned investigation. We report the results of 27-day long VHFR survey performed in the SCIR in February–March 2003 and compare our results with radar-derived circulation patterns along the Opal coast of France in the Dover Strait (Fig. 1).

The paper is organized as follows. In Section 2, we present the study site, environmental data recorded during the radar

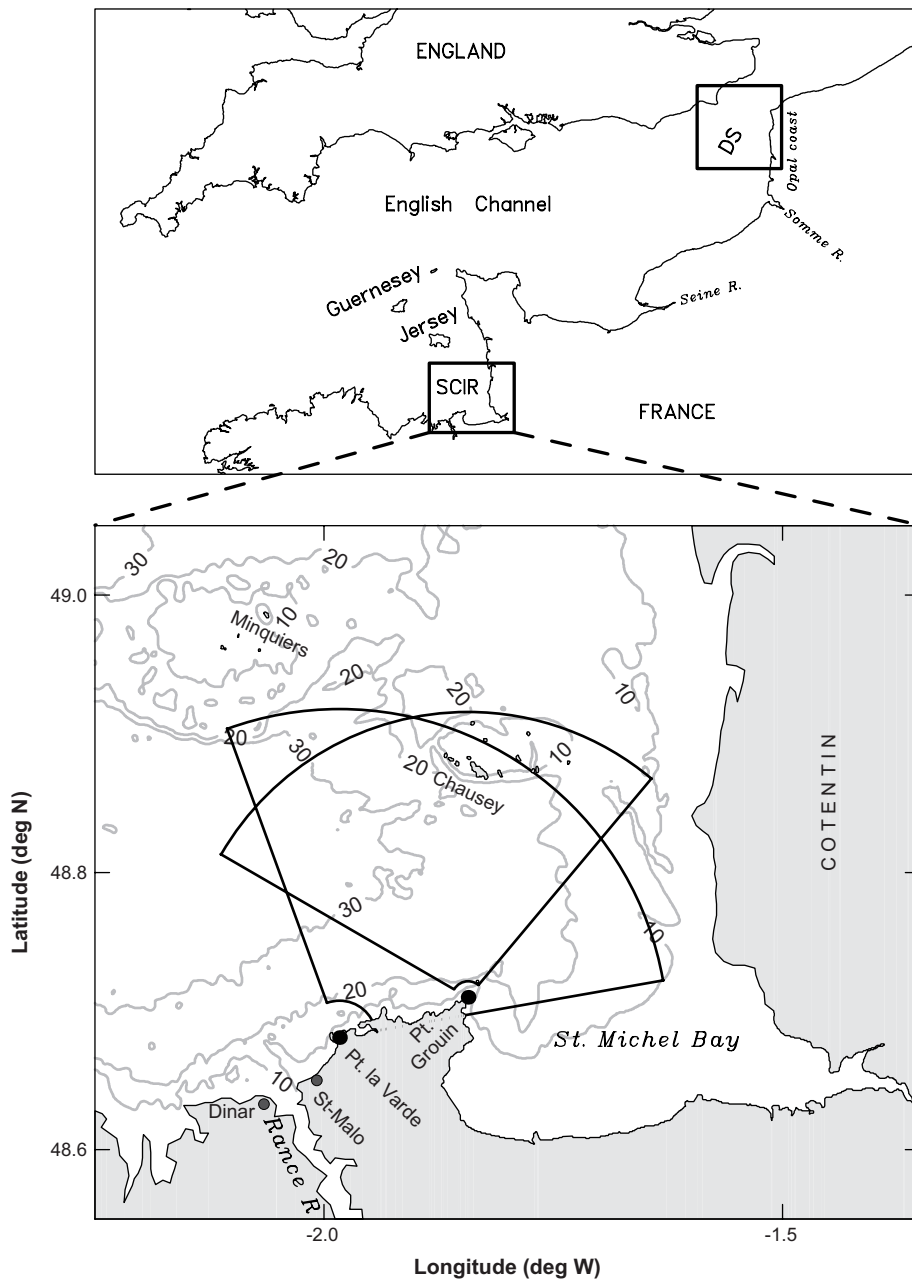


Fig. 1. Location of VHFR survey areas in the English Channel (upper panel). Experimental domain in the southern Channel Isles Region and radar coverage zone (lower panel). Radar sites are shown by black circles. Grey circles denote locations of geographic names used in the text. The Rance river contributing to the freshwater input, and bottom topography are also shown. Contour interval of bathymetry map is 10 m (grey solid lines).

experiment, VHFR configuration, and describe the sea surface current observations. In Section 3, the data are analyzed and the results are presented. The sea response to external forcing is decomposed into tidal and wind-driven components, and a long-term residual circulation pattern is reconstructed. Using the radar-derived surface current maps, we also estimated the mean Eulerian, Stokes and Lagrangian velocity fields across the region. Discussion of the results, comparison of current patterns in two different sites of the English Channel and conclusions are presented in Section 4.

2. Data and methods

2.1. Location of study site

The study site is located in the central part of the English Channel, south of the Channel Isles (Minquiers and Chausey), and is considered as the entry to the Mount Saint Michel Bay, referred hereafter as St. Michel Bay (Fig. 1). The SCIR is a partially enclosed, well vertically mixed body of water with extremely large tidal range, up to 13 m (second in the world). The coastline of the SCIR is highly irregular, with a large bay in the south-eastern part (St. Michel Bay) and numerous inlets. The water depth is less than 30 m in the majority of the SCIR. It gradually decreases eastward, yielding a several kilometre large shoaling area. In the middle of the domain, one can find Chausey, a group of small islands, islets and rocks that form part of the Channel Islands. The main island is 1.5 km long and 0.5 km wide, though this is just the tip of a substantial and complex archipelago which is exposed at low tide.

2.2. Environmental conditions

In the Channel Isles region, the tidal streams are rotary counter-clockwise, so near islands and islets a counter-clockwise transport is anticipated. This is due to reflection of the remotely forced tidal

waves arriving from the Atlantic ocean by the Cotentin Peninsular. The wave interaction occurring in a very shallow-water region is the dominant factor that determines variability of the sea surface height (SSH) and currents in the study area. The SSH variations range within 3–13 m, and the corresponding tidal currents reach 2 m/s. SSH variations in the port of St-Malo, located in the region of interest, are shown in Fig. 2a. The tidal signal has a predominant semi-diurnal period, with a pronounced fortnightly modulation due to the interference of the diurnal, M_2 , S_2 , N_2 , and semi-diurnal, M_4 , MS_4 constituents. Both primary and secondary spring tides occur during the period shown. The tidal velocities and transports show fortnightly variability in response to the spring–neap cycle.

Buoyancy forcing in the domain is weak. The majority of freshwater comes from Rance, Fremur and smaller rivers located on the southern coast. A peak total river discharge of 20 m³/s observed in January 2003 (<http://www.hydro.eaufrance.fr>) can be considered as negligible, compared to river discharge in the eastern English Channel (approximately 2000 m³/s) during the same period.

Fig. 2b shows the winds measured at the airport of Dinar during the experiment (Fig. 1). Two distinct wind regimes were observed. During the first 15-day period, winds were generally coming from the south with speeds ranging from 5 to 10 m/s. During the last 12-day long period, dominant winds were from the east.

2.3. VHFR data

The VHF radar system was developed at LSEET, University of South Toulon Var, France, two decades ago (Broche et al., 1987) and used in experiments in the Mediterranean Sea (e.g. Forget et al., 1990; Forget and Broche, 1991; Broche and Forget, 1993; Broche et al., 1998; Ivonin et al., 2004).

Two radars monitored surface currents in the SCIR from February 21 to March 24, 2003, in the framework of the research program EPEL-GNB of the French “Service Hydrographique et

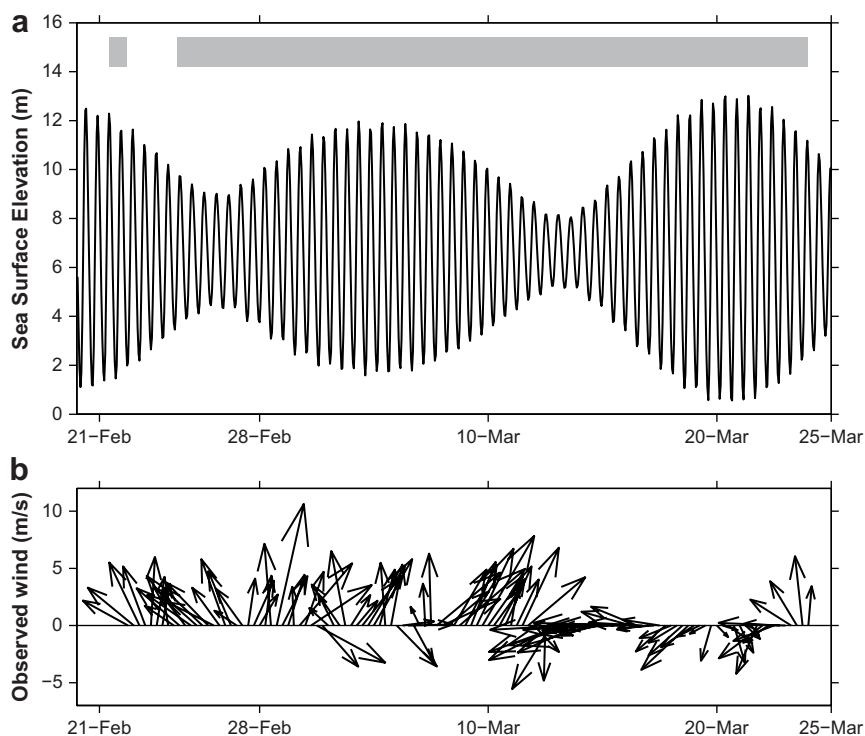


Fig. 2. External forcing data. (a) Tidal elevation observed in St. Malo during the experiment. (b) Wind measurements made at the airport of Dinar (Met-office data). Hourly data were averaged within 6 h for plotting. Time line of radial velocities available at both radar sites is shown by grey shading in (a).

Océanographique de la Marine" (SHOM). The program description is given at http://www.shom.fr/fr_page/fr_act_oceano/vagues/EPEL/epel_gnb_2003_f.html. One radar was located at the Point of Grouin (PGR), 30 m above the sea level. The other radar was located 11 km farther southwest at a flat-ground area of the Point la Varde (PLV), elevated by 25 m above the sea level (Fig. 1).

The radars operated at 45 MHz (PGR) and 47.8 MHz (PLV). Transmission is done by an endfire array of 4 antennas and reception by a broadside array of 8 equally spaced antennas stretched along 25 m parallel to the shoreline. The transmit array is perpendicular to the receipt array. Radial resolution was 600 m. The system provided a maximum horizontal range of 25–30 km. Radar signals were processed by beamforming (Broche et al., 2004). The azimuthal scanning provided ten beams with 10° discretization.

A typical operation scheme involves simultaneous 9 min of data acquisition from both sites followed by 12 min of data processing and standby. This sequence is repeated 2 times per hour and provides surface velocity vectors averaged over the 600 m radar cells at 30 min intervals. Summation of six consecutive Doppler spectra (incoherent summation) was performed to improve the data statistics. The basic integration time of 85 s provides the accuracy in radial velocity of the order of 4 cm/s. The statistics were improved further by averaging over three adjacent cells along each azimuth. Thus the effective radial resolution is 1.8 km. The resulting cell configuration is shown in Fig. 3.

Radial velocities were acquired by radars PGR and PLV at 99% and 93% of time, respectively. The chronology of measurements available at both radar sites reveals gaps on February 22–24 (Fig. 2a), caused by power supply failures at PLV site. Consequently, the 4-day period in the early part of the record has been excluded from consideration. A semi-automatic quality control has been applied to radial velocity data to remove the outliers and fill the gaps lasting less than 1.5 h (2-sample gaps). After that, in the area of signal overlap, the radial velocity data from two radar stations have been interpolated on a regular grid with 2 km spacing (Fig. 3) and

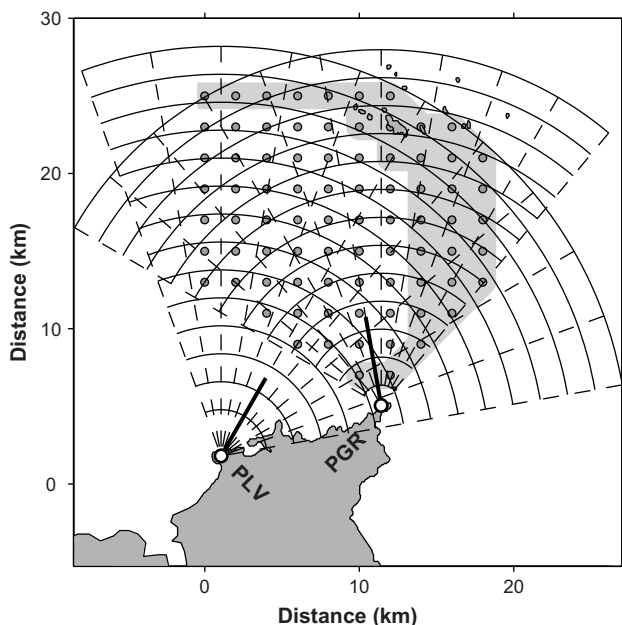


Fig. 3. The VHF radar coverage of the area with ten beams, each 10° wide, separated into "bins" of 1.8 km spacing and adopted after the along-beam averaging. The regular grid of 2 km spacing is shown by grey circles. Shading indicates the region where the vector data do not satisfy the quality control, and grid points inside this region were excluded from consideration. Radar sites are shown by open circles. Thick solid lines indicate the orientation of emitter antenna array on each radar site located at Point of Grouin (PGR) and Point la Varde (PLV).

combined to yield current velocity vectors. As a result, gridded surface velocity fields have been generated at 30-min intervals for a 27-day period from February 25 (00 h) to March 23, 2003 (24 h).

The data availability was high over the majority of the area with the data return approaching 100% in the central and western parts of the domain, and dropping off seaward eastward. The data quality at far ranges was poor because of the orthogonality of radar beams to dominant current direction and perturbations due to reflection by Chauvey. In addition, in the eastern part of the domain, the superposition of the forward and backward backscattered signal recorded at PLV site corrupted the quality of the data. Moreover, in the northern and eastern part of the radar coverage zone at far ranges, the beams intersect at small angles in a way that precision of the east–west Cartesian components of the current vectors are poor. This phenomenon, called the geometrical dilution of precision, was investigated e.g. by Chapman et al. (1997) and Shay et al. (2007). In our case, the precision on the west–east current components were estimated as 0.15 m/s, in the upper left grid cells in Fig. 3. These three arguments forced us to exclude edge grid cells (highlighted by shading in Fig. 3) from consideration.

2.4. Data analysis

We applied the EOF and principal component analysis (PCA) technique to this dataset in order to quantify the tidal flow dynamics over the period of interest. Parameters of synthesized ellipses, retrieved from the PCA, provide two major properties of tidal currents: the orientation and magnitude of the dominant current. The anisotropy of oscillatory tidal flow is quantified by estimating the ellipse eccentricity as the eigenvalue ratio of the velocity correlation tensor. The PCA technique does not give, however, information on the rotation of current vectors. To fill this gap, we applied a rotary analysis technique to velocity time series (Emery and Thompson, 1997). This involves the decomposition of the velocity vector into the clockwise (cw) and counter-clockwise (ccw) rotating circular complex-valued components. The rotary spectral analysis of 9-day long time series was performed to identify the dominant frequency in current velocity variation. This limited-length time series was generated by combining three successive 9-day long current velocity records. Both cw S_- (negative) and ccw S_+ (positive) power spectra revealed pronounced peaks at the semi-diurnal frequency. After that, the rotary coefficient, $r = (S_+ - S_-)/(S_+ + S_-)$, was estimated at every grid point using these peak values. r ranges from -1 for clockwise motion to $+1$ for counter-clockwise motion ($r = 0$ is oscillating non-rotational flow). In addition to the PCA, we also performed the EOF analysis which is particularly suitable for extracting weak but spatially coherent patterns hidden on the background of strong oscillatory tidal motion.

Harmonic tidal analysis by the least-squares method was performed separately for both components of the velocity time series using the technique developed at LEGOS, Midi-Pyrénées Observatory (Foreman, 1978). Nodal corrections were included in the determination of the tidal harmonics. Inference procedure was carried out for the astronomical constituents with frequencies less than Rayleigh resolution limit. We have used information on the amplitude and phase of the tidal constituents available from the historical data in the port of St-Malo. Four shallow-water constituents (M_4 , MS_4 , N_4 and M_6) were included in the analysis. The amplitude and phase of the constituents derived from the analysis were converted into standard parameters of tidal current ellipses.

We have also estimated the Eulerian, Lagrangian and Stokes components of the residual currents, and investigated the relationship between the residual currents and physical forcing recorded during the radar survey in the SCIR.

3. Results

3.1. Tidal currents: spatial patterns and variability

The evolution of tidal currents in time and space is quantified using the parameters of synthesized tidal current ellipses derived from the PCA and rotary spectral analysis applied to the velocity time series. The results are summarized in Figs. 4 and 5. Tidal current ellipses associated with a tidal wave arriving from the West correspond to the mean tidal flow conditions observed on March 17 (Fig. 4a). Ellipse orientation shows that currents are strongly controlled by the basin configuration and, to less extent, by the bottom topography which tends to align the major axes along the depth contours. One can distinguish anisotropy in current field with a relatively high ellipse eccentricity observed at far ranges

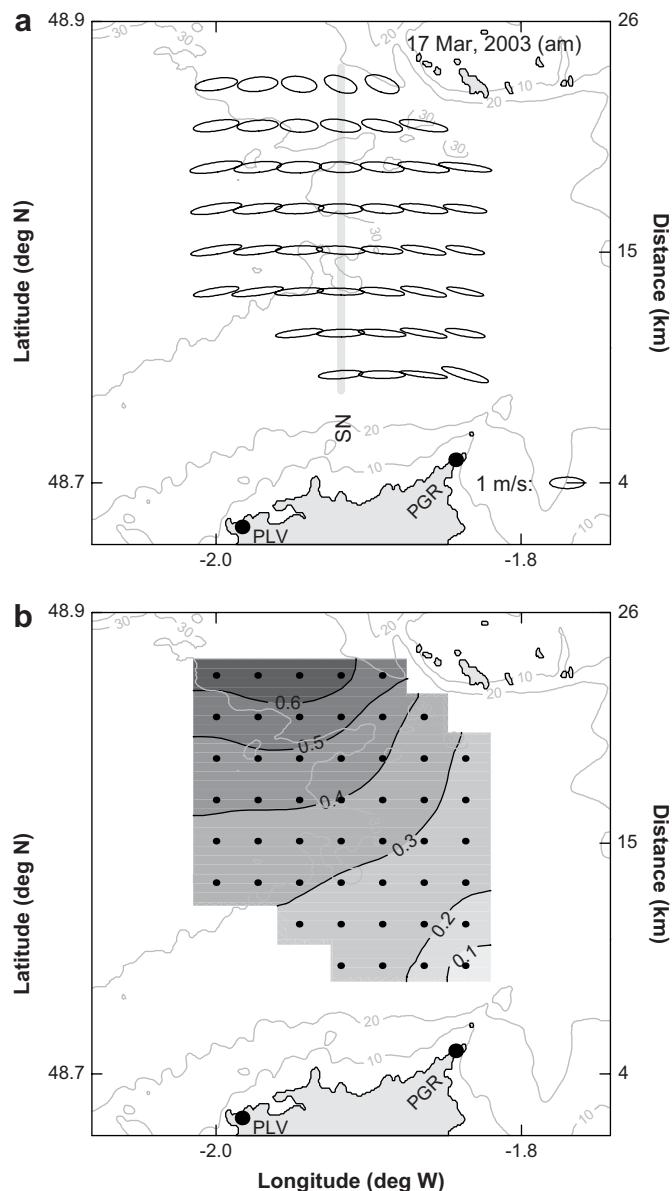


Fig. 4. (a) The PCA-derived tidal ellipses on March 17, 2003. Grey shading in the centre of the radar survey area indicates the position of the SN-line which contains eight grid points oriented in the cross-shore direction. (b) Contour plot of the rotary coefficient, r , derived through the rotary analysis of the velocity time series. r ranges from -1 for clockwise motion to $+1$ for counter-clockwise motion ($r = 0$ is unidirectional flow).

near Chausey. On this day, the current velocity reaches the maximum value of 1 m/s at a distance of 11–17 km from the coast, over the deepest part of the area of radar coverage. It should be noted that instrumental errors (beam-crossing angles close to limit at far ranges) might affect the spatial pattern of tidal current ellipse parameters. Since the ellipse shape to much extent depends upon the meridional velocity component (reconstructed with higher precision), we assume that instrumental errors have a limited effect on the spatial pattern of ellipse eccentricity.

The spatial distribution of rotary coefficient (Fig. 4b) shows that the currents are counter-clockwise (ccw) rotating with the maximum value of r (0.6) found in the northern part of the radar survey region. This maximum is caused by the current squash against the Chausey thus producing more circular shape of current ellipses (high eccentricity). In contrast, lower values, ranging from 0.1 to 0.2, are found in the south-eastern part of the domain, evidencing the bottom friction effect. Tidal stirring provides a complete homogenization of the water column over a broad shallow-water region and makes a contribution of the cw and ccw rotary components similar (ccw component is slightly higher). Consequently, surface currents have nearly rectilinear or reversing character at the entry of St. Michel Bay.

Fig. 5a shows evolution of the magnitude of tidal currents (semi-major axis of synthesized current ellipses) along a line oriented in the cross-shore S–N direction (SN-line, shown in Fig. 4a). Both primary and secondary spring tides can be recognized in the current velocity field. In the southern part of the line, the magnitude of tidal currents increases by more than 600% in 9 days, rising from less than 0.3 m/s on 12 March to 2.0 m/s on 21 March. The range of current variability is smaller (300%) in the northern sector, at grid points closest to Chausey. Pronounced fortnightly variability of the currents is caused by interaction between the major semi-diurnal and quarter-diurnal tidal constituents. The interference of M_2 and S_2 harmonics provides slightly less than two-thirds of this variability, whereas N_2 and the quarter-diurnal constituents, M_4 and MS_4 , also contribute by nearly a third of the total variability.

The current ellipse eccentricity does not show any pronounced fortnightly variability but exhibits strong variations in space (Fig. 5b). The values gradually increase northward from 0.1 to 0.2, in the vicinity of the coast, to 0.55, at the seaward margin of SN-line. The minimum value (0.1) is observed during the neap tide (14 March) 10–12 km offshore. We note one significant event which has been recorded between 10 and 13 March. During this period, eccentricity increased all over SN-line up to 0.5 and then dropped to 0.05–0.1. This event corresponds to a period when prevailing winds changed the direction from northern to western (Fig. 2b). Winds blowing from the East, in the direction parallel to the current ellipse orientation (ten-day period from 13 to 24 March) maintain relatively small values of eccentricity. Neap tide conditions (25–27 February and 13–14 March) seem to have similar effect on the eccentricity in the central part of the radar survey region where smaller values are observed. This rule does not apply at far ranges where eccentricity values are generally higher (near Chausey).

3.2. Tidal analysis

For a 27-day period of observations, the method of Foreman (1978) provides parameters for 20 tidal constituents of which three are derived by inferring: K_2 , T_2 in semi-diurnal and P_1 in diurnal clusters respectively. Fig. 6 shows tidal ellipses and Greenwich phase lag for the constituents M_2 and S_2 .

The tidal ellipses for the predominant M_2 constituent show homogeneous structure of the current with amplitudes ranging from 0.90 m/s (south-western sector) to 0.70 m/s at the level of Chausey. The direction of the maximum current (semi-major axis)

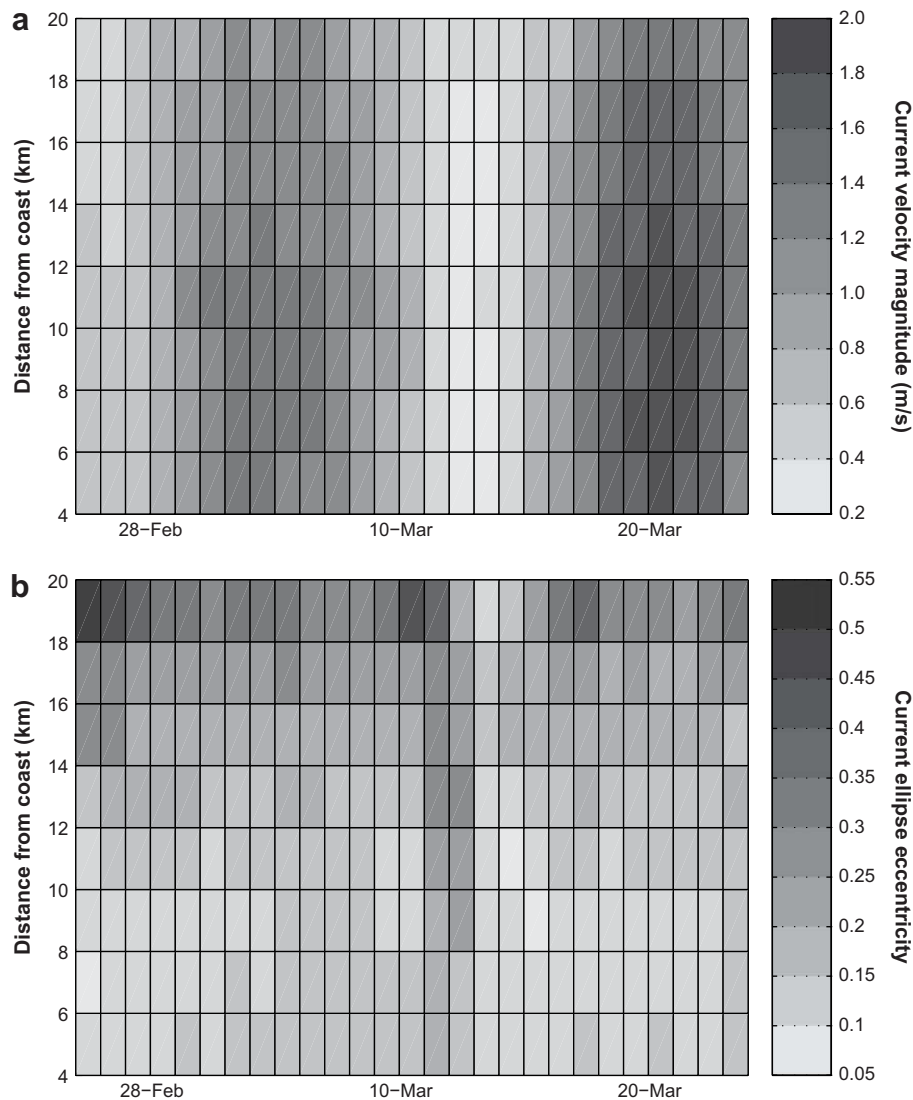


Fig. 5. Evolution of the amplitudes (a) and eccentricities (b) of tidal current ellipses over the experimental period along the SN-line (shown by grey shading in Fig. 4a).

veers cw following depth contours. The eccentricities with maximum value of 0.35 at the northern extremity (effect of Chau-sey islands) generally decrease southward to 0.05–0.1. The current vector rotation is ccw everywhere. The phase distribution shows the M_2 wave advance by up to 30° in the central part of the domain indicating faster propagation of the tide here.

The distribution of S_2 current ellipses and current phase is almost identical to that for M_2 with the amplitudes reduced by a factor of 0.40 and phase values shifted by approximately 50° . The rotation is again ccw. The S_2 wave propagation is faster in the middle of the Strait as shows the phase distribution.

Comparison of the phase distribution for elevation and currents reveals that they are approximately in quadrature. The phase of M_2 elevation in the SCIR ranges between 180° and 185° (Salomon and Breton, 1991; Davies et al., 1997), whereas the phase of the radar-derived currents is close to 70° on average (Fig. 6a). The corresponding values of phase for S_2 are respectively 235 – 240° for elevation (Davies et al., 1997) and 120 – 130° for currents (Fig. 6b). These features indicate that the water dynamics in the SCIR is dominated by a standing wave, responsible for filling and draining of the St. Michel Bay, and whose kinematics could be explained by tidal wave reflection by the Cotentin Peninsular.

3.3. Results of EOF analysis

Further insight on surface current pattern can be obtained from the EOF analysis, which is basically the velocity field expansion in the eigenmodes of its covariance matrix. The eigenvalue spectrum reveals only two statistically significant modes lying above the $n^{-3/2}$ power-law in a log–log plot of eigenvalue vs mode number n (Sirovich et al., 1995).

These two modes account for 97% of the variance in the dataset. Spatial structure of these modes and the corresponding amplitude time series are shown in Fig. 7. Current speeds for each of the two modes at time t can be calculated by multiplying a vector in the map (Fig. 7a and b) by the corresponding value $a(t)$ (Fig. 7c and d) and by the scale factor (0.025 and 0.005 respectively).

Mode 1 clearly dominates the spectrum accounting for 95% of the total variance of the surface velocity field. Evolution of its amplitude (Fig. 7c) strongly correlates with SSH recorded at the port of St-Malo (Fig. 2a). The amplitude of the first mode is an order of magnitude higher than that of the second EOF. Obviously, this mode of velocity field variation corresponds to tidal motions.

Fig. 7c clearly demonstrates that the curve of amplitudes of mode 1 has a pronounced asymmetry which could be related to

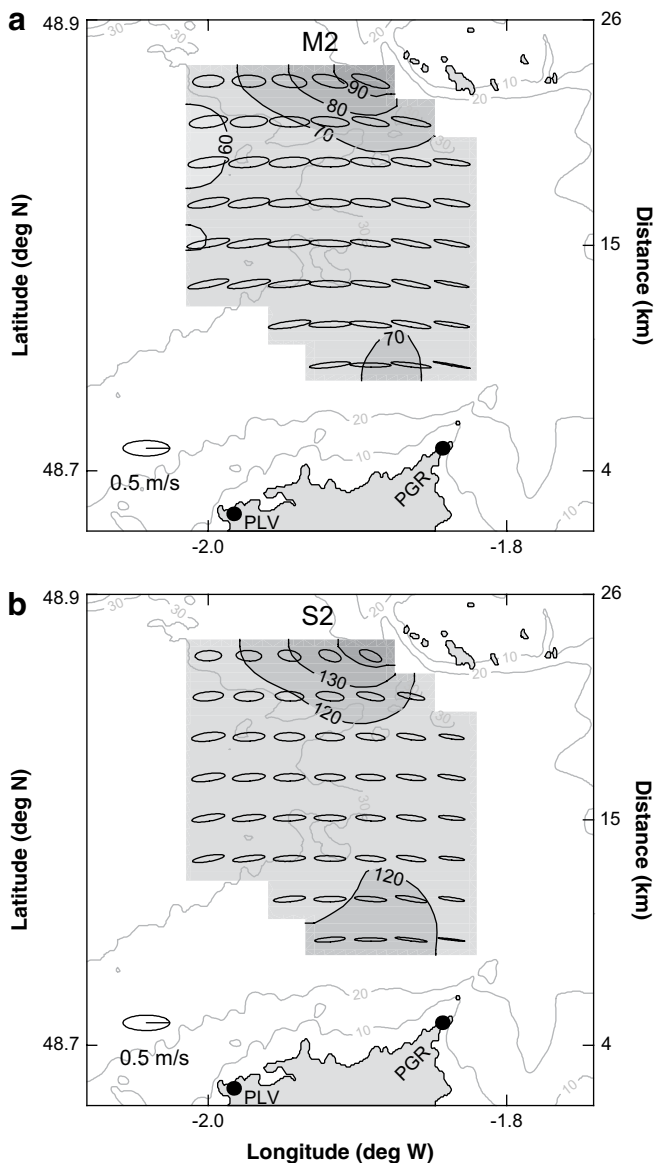


Fig. 6. Tidal current ellipses and phase for M_2 (a) and S_2 (b) tidal constituents. Phase distribution is shown by grey shading with contour intervals given every 10° . All ellipses are ccw polarized.

peculiarities of tidal wave propagation in the SCIR. To assess evolution of current field associated with mode 1, we have estimated the third and the fourth order statistical moments of the amplitude time series. The third order moment, skewness (s), provides the statistical measure of the asymmetry of distribution. The skewness is zero when the distribution is symmetric with respect to the mean value. Positive skewness characterizes distributions with a long tail in the range greater than the mean. The fourth order moment, kurtosis (k), gives an indication of the peakedness of the mode amplitude during a tidal cycle. Its value is 1.5 for a sinusoid. Furthermore, we have estimated the difference in duration of flood compared to ebb as a ratio $\epsilon = n_+/n_-$, where n_+ and n_- are the number of positive and negative values of amplitude $a(t)$, within a period of analysis.

Table 1 shows that asymmetry is observed during the whole period of observations, under different tidal conditions and wind forcing. The asymmetry arises from the difference in duration of flood compared to ebb. On average, the duration of flood (eastward

currents) is smaller than that of ebb ($\epsilon = 0.83$), but its intensity (peak current velocity) is larger ($k = 2.4$). For positive values of $a(t)$, the curve of amplitudes is sharp. It is conversely flattened when the amplitude reaches extreme negative values and shows a tail at negative $a(t)$. Fortnightly tidal cycle tends to modify the asymmetry of the mode 1 amplitude (ϵ ranges from 0.75 to 0.88) showing a noticeable (17%) variation in duration of ebb compared to flood (Table 1). The difference in intensity of the current velocity over a tidal cycle shows stronger (47%) fluctuations within the same period (k ranges from 1.7 to 2.5).

Local winds might also have a strong effect on the evolution of the currents by enhancing the asymmetry of the curve (s and k), intensifying flood currents by 31%, and increasing the duration of ebb by 13%. Specifically, it concerns westward winds parallel to velocity vectors of mode 1. The values of $a(t)$, averaged over specific periods (last column in Table 1), follows the evolution of ϵ and k and provides an additional evidence that the direction of the mean tidal flow might change according to phases of tidal period or local atmospheric forcing, e.g. two dominant wind regimes shown in Fig. 2b and listed in Table 1.

The vector field of mode 2 reveals the existence of a cyclonic eddy-like structure north-west of the Point of Grouin, and a current intensification west of Chausey (Fig. 7b). Both structures are only partially captured by the radars. Whereas eddy formation can be attributed to interaction of the strong east-west oriented tidal flow with PGR (Pingree and Maddock, 1985b), the origin of current intensification in the north of the radar survey region is not so evident. It might be a part of another large eddy centered on Chausey.

Time variation of the mode 2 amplitude (Fig. 7d) shows the dominant contribution of tidal motions. Strong semi-diurnal variability of the signal is modulated by the fortnightly tidal cycle. Correlation (c) with the wind is also visible. Specifically, the E-W winds, dominating during the last ten days of the experiment, tend to modulate the magnitude of mode 2 at low frequency ($c = 0.68$). In contrast, at the beginning of the experiment, the dominant S-N component, and oscillating character of winds, produce smaller effect on mode 2 ($c = 0.53$).

3.4. Residual currents

The field most relevant for the transport of material in sea environment is the residual circulation (RC). It is of a primary importance in tidally energetic basins such as the English Channel where the propagation of tidal energy from the North Atlantic produces a significant residual flow (Salomon and Breton, 1991). The Eulerian description of the mean flow is most convenient as it is directly obtained from by averaging horizontal surface velocities provided by the radars.

Fig. 8a and b shows residual velocities estimated by averaging the monitored surface currents over two consecutive periods of 15-day and 11-day long. Prevailing winds (Fig. 2b) were from the southern sector during the first period (25 Feb–11 Mar) and from the eastern sector during the second period (12–22 Mar). The resultant current field includes tidally induced, wind-driven, and other components of non-tidal origin. Averaging the surface currents over the whole period of observations provides a current field similar to that of Fig. 8a.

The figure reveals strong control of the RC by topographic features and basin configuration. Specifically, one can see a transverse circulation induced by a tidal current ascending the bottom slope. A noticeable contribution of wind to the residual flow is also detected. The mean flow shown in Fig. 8a (and also the 27-day averaged mean flow), has globally northward orientation over the majority of the domain with the velocity magnitude up to 12 cm/s.

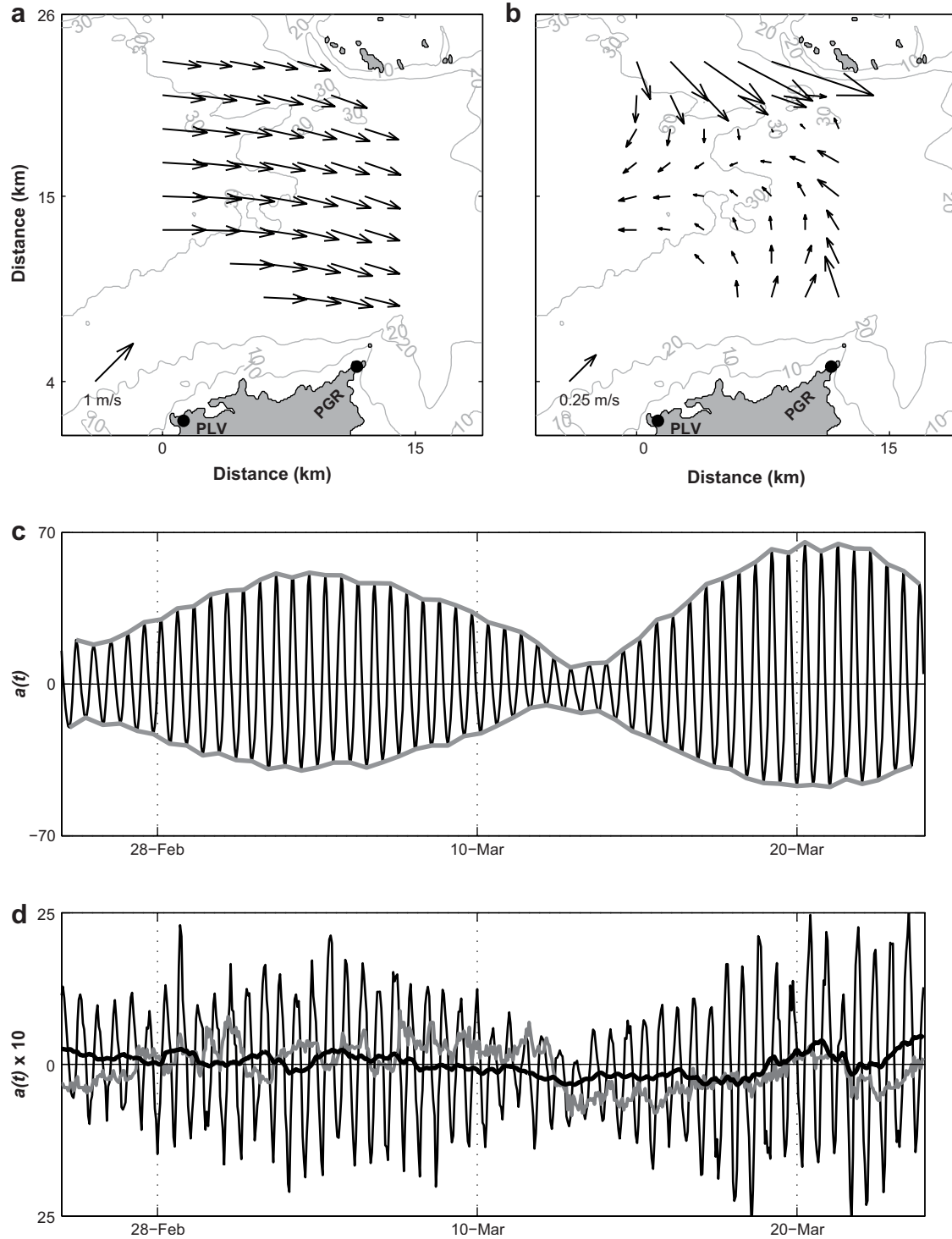


Fig. 7. The EOF vector maps for modes 1 (a), 2 (b), and amplitude time series for modes 1 (c) and 2 (d). Bold grey line in (d) is the E–W component of the wind, and bold black line is low-pass filtered mode 2 amplitude time series.

Current vectors turn west-north-west at far ranges and east-north-east south of Chausey, evidencing the effect of islands. In these two places the currents become weaker. Winds from the eastern sector, dominating the second period of observations, tend to reinforce the western component of the mean flow (Fig. 8b).

In a more rigorous way, the nature of the wind response was examined statistically by assuming the following relation for the (non-tidal) residual times series (Prandle and Matthews, 1990),

$$R(t) = \bar{R} + \alpha\tau(t - \Delta t) \tag{1}$$

where \bar{R} is the steady non-wind-driven residual current, Δt is a time lag between wind and surface current response, and α is a complex-valued coefficient. τ is the wind stress calculated from the hourly wind data and assumed to be power-law function of the wind speed W^n . The complex current vector $R(t)$ was derived from low-pass filtered VHFR surface current velocities. The filter reduces tidal

Table 1

Estimates of skewness (s), kurtosis (k), ratio (ϵ) of the number of positive to negative values of the amplitude of mode 1, and the average amplitude ($\langle a \rangle$) at different periods of the experiment. ϵ has the sense of duration of flood compared to ebb, whereas k matches the intensity (peak velocity) of currents during a tidal cycle.

Period of time	s	k	ϵ	$\langle a \rangle$
Primary spring tide (17–23 Mar)	0.3	1.7	0.85	0.5
Neap tide (9–16 Mar)	0.3	2.5	0.75	–1.2
Secondary spring tide (1–8 Mar)	0.3	1.7	0.88	1.0
Northward winds (28 Feb–11 Mar)	0.3	1.9	0.87	0.9
Westward winds (12–22 Mar)	0.5	2.5	0.77	–0.7
Whole period (25 Feb–23 Mar)	0.4	2.4	0.83	0.0

(diurnal, semi-diurnal) and inertial variability to less than 1% of their original values, and passes 90% or more of the desired signal (Stacey et al., 1986). The wind data were smoothed by 12-h moving average which eliminates high-frequency oscillations. The values of \bar{R} and α were calculated by least-squares fitting for different powers of the wind speed, W , and time lag, Δt , assumed. The overall correlation between the observed and estimated residual velocities (formula 1) were not especially sensitive to neither time lag (in the range 0–6 h) nor to the power of the wind speed. The maximum correlation, 0.98, was found for a time lag of 1 h and $\tau \propto W^2$, with the error (rms) of current estimation of the order of 3 cm/s.

The spatial pattern of \bar{R} is shown in Fig. 8c. The RC field reveals a dominant northward flow over the majority of the VHFR-surveyed region with current magnitudes ranging from 2 to 8 cm/s. Qualitatively, this field is similar to residual circulation obtained by averaging of surface currents over the first 15-day long period (Fig. 8a), and during the whole period of observations (not shown), but the velocities are lower. The velocity vectors are aligned along the depth contours over the majority of the domain. At far ranges, zonally oriented residual flows are detected. Spatial distributions shown in Fig. 8a–c demonstrate complexity of the RC in the SCIR and the effect of Chausey on the residual flow. The values of α , subsequently reduced by bottom friction in shallower water, and \bar{R} have been used to calculate a long-term time-dependent RC by subtracting the rhs of (1) from the observed surface currents. The variability of the long-term residual currents at the cross-shore section (SN-line) is shown in Fig. 8d. The figure reveals a low-frequency modulation of the RC, a rotational character of the flow, and the change in sign of rotation during the period shown.

At the beginning of the record, around the neap-tide period centered on 25 February, there are dominant offshore flows with higher speed (up to 8 cm/s) observed on the northern and southern boundaries of the domain. Starting from 1 March, four RC reversals have been recorded. They correspond to a secondary spring-tide period (Fig. 2a) centered on 5 March. The sign of vector rotation changes during this period from cw, at the beginning, to ccw, at the end. Two significant events are recorded during the following neap- and spring tide periods. Firstly, there is a well-defined intensification of the cross-shore currents at neap tide with flow speeds up to 10 cm/s observed approximately 3–7 km from the shore. On the northern and southern margins, the direction of RC is opposite (Fig. 8d). During the primary spring tide centered on 20 March, the velocity field is completely different. The northward cross-shore flow dominates over the majority of SN-line. The rotation of current vectors is cw, and its speed does not exceed 6 cm/s. Close to the coast and in the vicinity of Chausey, the rotation of current vectors is rather instable, it often changes the sign from cw to ccw. Variability of residual currents observed in Fig. 8d gives an indication for a probable control of the long-term RC by fortnightly tidal cycle. Specifically the effect of primary spring or neap tides can be clearly identified. On the contrary, during the secondary neap–spring cycle, the RC variability seems to be more

irregular, showing a frequent change of current speed and direction. The magnitudes of time-independent (Fig. 8c) and time-dependent long-term RC along the SN-line (Fig. 8d) are comparable.

It is necessary to note that the residual velocities shown in Fig. 8a–c are not those that a passive material might be expected to follow. The Lagrangian velocity is more appropriate measure of the rate of passive particle displacement in the spatially non-uniform flow field and should be used for estimating a long-term transport and dispersion of material in the oscillatory tidal flows (Salomon et al., 1995; Bailly du Bois and Dumas, 2005). These two velocities are generally different, depending on spatial gradients of the velocity field (Pingree and Maddock, 1985a; Zimmerman, 1986).

The difference between the Eulerian and Lagrangian velocity fields, known as the Stokes velocity \mathbf{v}_s , can be estimated as $\mathbf{v}_s = \langle (\mathbf{v} \cdot \nabla) \mathbf{v} \rangle$, where brackets denote time integration over the period of observations. Using the sequence of 1296 surface velocity maps we have estimated the mean \mathbf{v}_s (Fig. 9a). The resultant field reveals a weak shoreward ccw rotating Stokes drift with velocity magnitude ranges between 1.5 and 5 cm/s. Higher values of Stokes velocity (5 cm/s) are found in the southern sector of the domain, indicating stronger horizontal gradients in the flow field in the vicinity of the shore.

The Lagrangian velocity field, determined as the sum of Eulerian and Stokes velocities ($\mathbf{v}_L = \mathbf{v}_E + \mathbf{v}_s$), is shown in Fig. 9b. This field differs from the Eulerian residual velocities (Fig. 8a). The current magnitude ranges from 1 to 10 cm/s and shows a central jet in the north-west direction. The current speed decreases both onshore and offshore from the axis of the jet. A weak flow convergence is present in the Lagrangian velocity field in the northeastern part of the radar survey region.

4. Discussion and conclusions

The experiment reported in this paper involved the first use of a VHF radar system to study circulation in highly energetic tidal basin – the southern Channel Isles region. The radar-derived surface currents were investigated by means of various numerical and statistical techniques (principal component, rotary, EOF, and harmonic analyses). The primary insights are based on high resolution of the VHFR data, in both temporal and spatial dimensions, which provides significant level of confidence in the observed surface flow patterns. The data reveal flow complexity and its variability at a level of details that were not previously available. Though there have been a number of important modeling studies of circulation in the SCIR (Pingree et al., 1985; Le Hir et al., 1986; Salomon and Breton, 1991), the presented radar survey has brought a significant contribution to understanding physical processes governing the coastal water dynamics in the region where the tidal range is one of the highest in the world. The acquired data could be very useful for coastal circulation model validation and initialization, comprehension and interpretation of remote sensing images (Pingree et al., 1985), and also for studying specific issues such as sediment dynamics in the region of St. Michel Bay.

The circulation in the SCIR is completely dominated by tides. The wind effect on the flow is less important, while the buoyancy forcing is negligible. This makes the local circulation noticeably different from that observed by oceanographic coastal radars in other regions of the English Channel (Prandle et al., 1993; Sentchev and Yaremchuk, 2007) and the North Sea (Matthews et al., 1993; De Valk, 1999; Carbajal and Pohlmann, 2004). The major difference involves polarization of tidal currents. In the SCIR, the radar-derived currents are ccw polarized (Fig. 4b). This feature is related to the property of tidal flow which tends to follow the behavior of the Kelvin wave and its reflection by the Cotentin Peninsular.

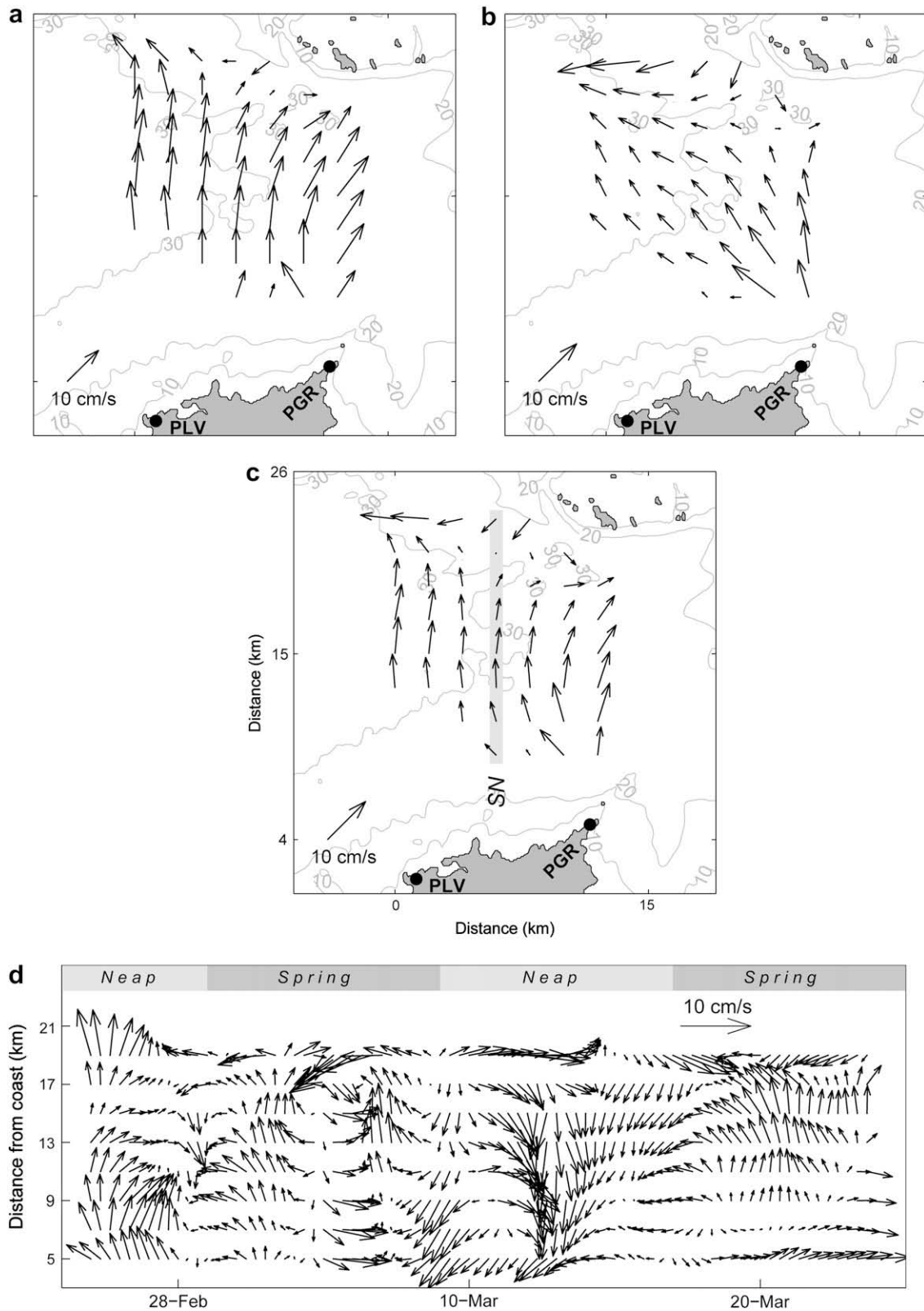


Fig. 8. (a) Observed surface currents averaged over the 15-day period at the beginning of the experiment (25 February–11 March, 2003). (b) Currents averaged over the last 11-day period (12–22 March, 2003). (c) Steady residual currents with the wind-driven component removed. (d) Long-term time-dependent surface residuals along the SN-line (shown by grey shading in (c)).

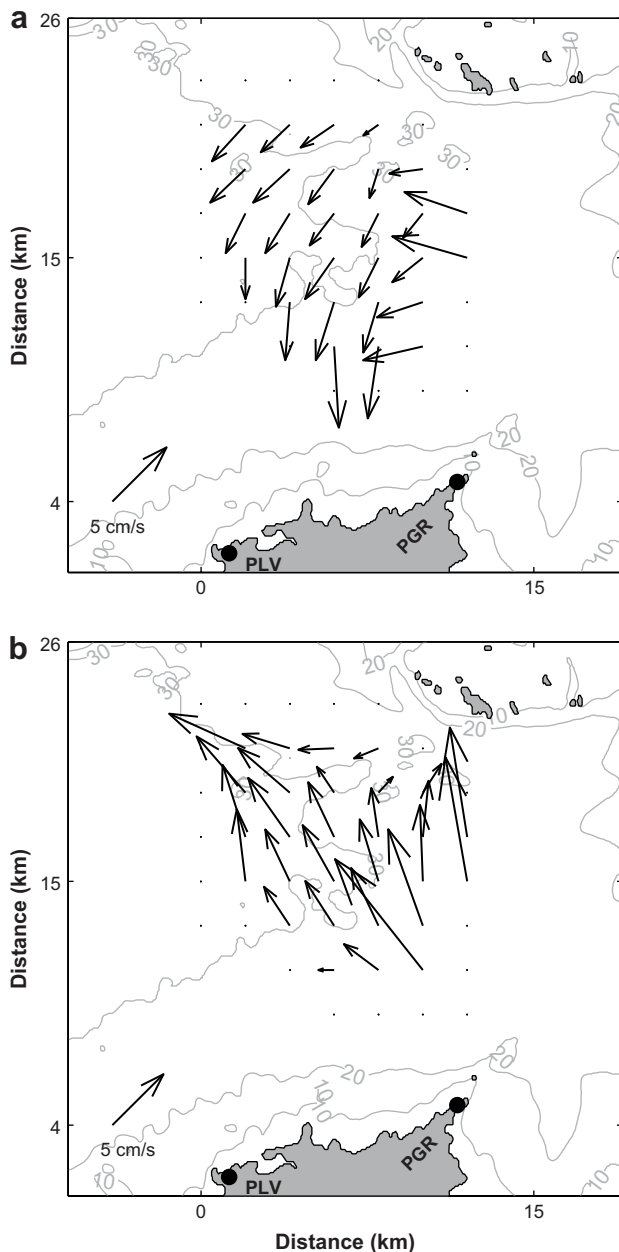


Fig. 9. The estimated Stokes (a) and Lagrangian velocity field (b).

Conditions indicating ccw rotation of current ellipses can be deduced from tidal charts (Prandle, 1982; Carbajal, 2000). Homogeneous spacing and orthogonality of co-tidal lines in the SCIR, documented by Salomon and Breton (1991), Sentchev et al. (2006), support the hypothesis of the ccw rotation of current ellipses in this region. Drifting buoy tracking, performed in 1983 in the Channel Isles region south of Jersey (Pingree et al., 1985), provides an additional support for ccw current vector polarization. The Kelvin wave reflection in coastal ocean regions has been investigated by many authors, e.g. Hendershott and Speranza (1971) in the Adriatic Sea and Gulf of California; Malačić et al. (2000), Janeković and Kuzmić (2005) in the northern Adriatic; Carbajal and Pohlmann (2004) in the southern North Sea. In all these regions, the ccw current vector rotation has been documented.

In contrast to the SCIR, polarization of tidal currents in the Dover Straits and along the northeastern coast France changes from ccw nearshore to cw farther offshore, indicating a transition from

a vertically homogeneous to stratified structure of the water column. Stratification is induced by the freshwater input from a number of rivers (Seine, Somme and others) and assumed to be responsible for surface current convergence on ebb, divergence on flood, and strong oscillatory vertical motion. Spectral analysis of the observed currents and the results of the Agro drifter tracking indicate that the line of current convergence approximately follows the 30-m isobath (Sentchev and Yaremchuk, 2007). Similar features of tidal current ellipse polarization were observed in other regions of the North Sea affected by the freshwater discharge (Visser et al., 1994; Carbajal and Pohlmann, 2004).

EOF analysis of the VHFR data has shown that the first two EOF modes account for 97% of the variance, with the major contribution of the first mode. This mode accounts for oscillating tidal currents, whereas the second mode represents motions emerging from the interaction of tidal currents with capes and islands. The spatial structure of the modes shows a strong control of surface currents by the bottom topography, and a number of small scale features in the current field hidden under the background of the powerful tidal circulation. It is likely that the eddy (more precisely a part of the eddy) detected in the southwestern part of the radar coverage zone (Fig. 7b) is the result of interaction of the strong east-west oriented tidal flow with the cape (PGR). During the ebb (westward flow), positive vorticity is generated thus contributing to formation of a ccw eddy. The flow field of mode 2 shown in Fig. 7b is relevant to this phase of the tidal cycle. During the flood, the same mechanism produces a cw rotating eddy. The dynamics of eddies, generated by the interaction of tidal current with capes and promontories, have been studied numerically by Signell and Geyer (1991), Park and Wang (2000). Geyer and Signell (1990) used a ship-board ADCP to map the structures of a tidal eddy off the Massachusetts shore. These studies have shown consistency of model results with observations and suggested that topographic vorticity tendency and water column stretching could be the dominant forcing terms in the production of transient tidal vorticity.

The oscillating jet detected by the radars in the northern sector of the SCIR is caused by interaction of the ccw rotating tidal currents with the Chausey Islands. Our results are consistent with the numerical study performed by Pingree and Maddock (1985b). The limited spatial extension of the VHFR data did not allow to shape the entire structure the currents south of the Chausey. However the jet in Fig. 7b provides an indication of the existence of a rotary ccw tidally induced residual flow around the islands (Pingree and Maddock, 1985b).

Current patterns of both modes oscillate at semi-diurnal frequency (Fig. 7c and d). A fortnightly variability of the modal amplitudes is found as well. The latter creates situations with relatively weak (0.2–0.4 m/s) flow, growing up to 2 m/s during the next six-day period. This exceptional (about 600%) variability of currents in the SCIR is well captured by the VHFR observations (Figs. 5 and 7). The magnitude of fortnightly variation of tidal currents is caused by interaction between the major semi-diurnal and quarter-diurnal tidal waves propagating in the SCIR. The interference of M2 and S2 harmonics provides nearly two-thirds (380%) of this variation. The contribution of the N₂ and the quarter-diurnal constituents, M4 and MS4, is also considerable; in total they account for a third of it (140% and 70% respectively). The authors did not find in literature any results (experimental or modeling) relevant to such variability of tidal currents in other coastal ocean regions.

The statistical analysis of mode 1 amplitude time-series revealed a strong asymmetry of the current velocity curve which indicates that tidal circulation in the SCIR is flood-dominated, i.e. period of flood is shorter but flood currents are more intense than ebb currents. We have also demonstrated that wind events and

fortnightly variability might affect the structure of tidal cycle by modifying the magnitude and duration of ebb and flood, i.e. provide more distortion of level and velocity curves. We note that at neap tides, the rising water level and currents have sharper peaks, then decrease slowly (most slow before low water), until rising rapidly as the tide comes. Westward winds have the same effect. At spring tides, durations of ebb and flood are comparable producing a more symmetric current curve.

Statistical moments of mode 1 amplitudes, summarized in Table 1, allowed us to estimate variations in duration of ebb and flood in response to various forcing components as 13% for wind, and 17% for fortnightly tidal cycle. Corresponding variations in current intensity are estimated as 31% and 47%. The asymmetry of tidal curve has been documented by many authors in different shallow-water coastal or estuarine environments (Aubrey and Speer, 1985; Blanton et al., 2002; Huang et al., 2008). This asymmetry in water level and velocity curves is caused by non-linearities due to bottom friction and basin morphology generating shallow-water tidal constituents. The distortion of the tidal and tidal current curves plays an important role in sediment transport (Ridderinkhof, 1997), and is of primary importance for St. Michel Bay which has a tendency to be silted up.

The temporal mean field inferred from the VHFR data, contains a signature of a cross-shore flow with the maximum velocity of the order of 12 cm/s (Fig. 8a and b). This field includes tidally induced, wind-driven, and other components of non-tidal origin. The regression analysis of the residual velocity time series (with tidal component removed) provided an estimate of the stationary residual surface current field and the wind-driven response. A well-defined cross-shore stationary surface flow is observed over the majority of the domain with the maximum velocities of 8 cm/s (Fig. 8c). Qualitatively, our results are consistent with estimates of the Eulerian residual velocities from numerical modeling (Orbi and Salomon, 1988) and from the analysis of current records in the SCIR (Le Hir et al., 1986). A transverse circulation induced by a tidal current escalating the depth gradient was emphasized by Godin (1988). He showed that depth gradients and bottom friction tend to veer the RC to the left of the direction of tidal wave propagation (in the northern hemisphere), and make it parallel to the depth contours. The presence of Chausey affects the residual circulation and splits the flow into two branches of opposite direction: westward and eastward.

A long-term, time-dependent, component of residual currents have been also estimated from the analysis of residual velocity time series. Specific features of this component are low-frequency modulation by fortnightly cycle, rotational character of the flow, and change in sign of rotation during the period of observations. Our results have also shown that the magnitudes of time-dependent and stationary residual currents are comparable. This allows us to assume that under favorable conditions (e.g. primary neap-tide conditions) the residual flow velocity might change considerably, until decreasing to zero.

We have performed both the Eulerian and Lagrangian estimates of the residual velocity fields. Formally, the Lagrangian description is the most relevant for the purpose of the transport diagnostics. This velocity field was estimated in the English Channel using Lagrangian tracking approach (Sentchev and Korotenko, 2005), Lagrangian barycentric method (Orbi and Salomon, 1988), or conventional modeling technique (Pingree and Maddock, 1985a). In the SCIR, the pseudo-Lagrangian tracking in the radar-derived velocity field is not applicable because the size of the domain is less than the tidal excursion length. On the other hand, we estimated the difference between the Eulerian and Lagrangian velocity fields, known as the Stokes velocity v_s (Fig. 9a). The resultant field is ccw rotating and reveals a moderate (maximum value is 5 cm/s)

shoreward Stokes velocity suggesting that the two quantities of the flow field, Eulerian and Lagrangian, are not equal here. According to Pingree and Maddock (1985b), Stokes flow near the coastline has the same sense as the far field rotary flow. In the SCIR, the tidal flow is ccw-rotating and the velocity field presented in Fig. 9a is in complete agreement with these considerations. Since the Stokes velocity is linearly related to the net energy flux (Prandle et al., 1993), the shoreward veering of v_s may also be interpreted as a consequence of stronger interaction of tidal currents with bottom topography near the PGR. This interaction may cause enhanced dissipation of tidal energy and, as a consequence, convergence of the net energy flux.

We conclude that the analysis applied to the VHFR data provided a useful examination of spatial and temporal variability of surface circulation in the SCIR, and were fairly useful in extracting meaningful flow patterns: tidal circulation, stationary and time-varying residual flow, and also tidally generated small-scale structures such as eddies and jets. To quantify physical mechanisms governing the regional circulation further research is needed. These studies would require a combination of the remotely sensed VHFR observations with *in situ* data collected during the EPEL-GNB project. To provide the best efficiency for future monitoring, the merged data sets should be synthesized with dynamical information supplied by numerical coastal models in the framework of the data assimilation technique. Implementation of this approach is a subject of our further research.

Acknowledgments

The field campaign was conducted in the framework of EPEL-GNB scientific project. We would like to thank Fabrice Arduin (SHOM/CMO/RED) for providing VHFR data. The authors are indebted to Jean-Charles De Maistre, Joel Gaggelli (LSEET) and ACTIMAR Company for their contribution to the field experiment, and to Pr. Pierre Broche (LSEET) for participation to radar data processing and interpretation. We acknowledge Laurent Reblou and Florent Lyard (LEGOS) for their interest to our work and providing recommendations relating to the data analysis.

References

- Aubrey, D., Speer, P., 1985. A study of non-linear tidal propagation in shallow inlet/estuarine systems Part I: observations. *Estuarine Coastal and Shelf Science* 21, 185–205.
- Bailly du Bois, P., Dumas, F., 2005. Fast hydrodynamic model for medium- and long-term dispersion in seawater in the English Channel and southern North Sea, qualitative and quantitative validation by radionuclide tracers. *Ocean Modelling* 9, 169–210.
- Bassin, C.J., Washburn, L., Brzezinski, M., McPhee-Shaw, E., 2005. Sub-mesoscale coastal eddies observed by high frequency radar: a new mechanism for delivering nutrients to kelp forests in the Southern California Bight. *Geophysical Research Letters* 32.
- Blanton, J.O., Lin, G., Elston, S.A., 2002. Tidal current asymmetry in shallow estuaries and tidal creeks. *Continental Shelf Research* 22, 1731–1743.
- Breivik, O., Sætra, O., 2001. Real time assimilation of HF radar currents into a coastal ocean model. *Journal of Marine Systems* 28, 161–182.
- Broche, P., Barbin, Y., de Maistre, J.C., Forget, P., Gaggelli, J., 2004. Antennas processing and design for Vhf “COSMER” coastal radar. In: *Proceeding of the “Radiowave Oceanography Workshop ROW-4”*, CDROM, Townsville, Australia, 21–23 April 2004.
- Broche, P., Forget, P., 1993. Shallow water waves observed by a VHF ground-wave Doppler radar. *International Journal of Remote Sensing* 14, 2301–2314.
- Broche, P., Devenon, J.L., De Maistre, J.C., Forget, P., 1998. Experimental study of the Rhône river plume. *Physics and dynamics. Oceanologica Acta* 21 (6), 725–738.
- Broche, P., Forget, P., De Maistre, J.C., Devenon, J.L., Crochet, M., 1987. VHF radar for ocean surface current and sea state remote sensing. *Radio Science* 22, 69–75.
- Carbajal, N., 2000. A criterion to locate regions with anticyclonic tidal current rotation. *Continental Shelf Research* 20, 281–292.
- Carbajal, N., Pohlmann, T., 2004. Comparison between measured and calculated tidal ellipses in the German Bight. *Ocean Dynamics* 54, 520–530.
- Chapman, R.D., Shay, L.K., Graber, H.C., Edson, J.B., Karachintsev, A., Trump, C.L., Ross, D.B., 1997. On the accuracy of HF radar surface current measurements:

- intercomparisons with ship-based sensors. *Journal of Geophysical Research* 102, 18737–18748.
- Davies, A.M., Kwong, S.C.M., Flather, R.A., 1997. A three dimensional model of diurnal and semi-diurnal tides on the European shelf. *Journal of Geophysical Research* 102 (C4), 8625–8656.
- De Valk, C.F., 1999. Estimation of 3-D current fields near the Rhine outflow from HF radar surface current data. *Coastal Engineering* 37, 487–511.
- Emery, W.J., Thompson, R.E., 1997. *Data Analysis Methods in Physical Oceanography*. Pergamon, NY, 634 pp.
- Foreman, M.G.G., 1978. *Manual for Tidal Currents Analysis and Prediction*. Pacific Marine Science Report 78-6. Institute of Ocean Sciences, Patricia Bay, 57 pp.
- Forget, P., Broche, P., 1991. A study of VHF radio wave propagation over a water surface of variable conductivity. *Radio Science* 26, 1229–1237.
- Forget, P., Devenon, J.L., De Maistre, J.C., Broche, P., Leveau, M., 1990. VHF remote sensing for mapping river plume circulation. *Geophysical Research Letters* 17, 1097–1100.
- Geyer, W.R., Signell, R., 1990. Measurements of tidal flow around a headland with a shipboard acoustic Doppler current profiler. *Journal of Geophysical Research* 95, 3189–3197.
- Godin, G., 1988. Tides. CICESE, Ensenada B.C., Mexico.
- Haus, B.K., Wang, J.D., Rivera, J., Smith, N., Martinez-Pedraja, J., 2000. Remote radar measurement of shelf currents off Key Largo, Florida. *Estuarine Coastal and Shelf Science* 51, 553–569.
- Hendershott, M.C., Speranza, A., 1971. Co-oscillating tides in long narrow bays, the Tailor problem revised. *Deep-Sea Research* 18, 959–980.
- Huang, H., Chen, C., Blanton, J.O., Andrade, F.A., 2008. A numerical study of tidal asymmetry in Okatee Creek, South Carolina. *Estuarine Coastal and Shelf Science* 78, 190–202.
- Ivonić, D.V., Broche, P., Devenon, J.-L., Shrira, V., 2004. Validation of HF radar probing of the vertical shear of surface currents by ADCP measurements. *Journal of Geophysical Research* 109, 1–8.
- Janeković, I., Kuzmić, M., 2005. Numerical simulation of the Adriatic Sea principal tidal constituents. *Annales Geophysicae* 23, 3207–3218.
- Kaplan, D.M., Largier, J.L., Botsford, L.W., 2005. HF radar observations of surface circulation off Bodega Bay (northern California, USA). *Journal of Geophysical Research* 110, C10020, doi:10.1029/2005JC002959.
- Kosro, P.M., 2005. On the spatial structure of coastal circulation off Newport, Oregon, during spring and summer 2001 in a region of varying shelf width. *Journal of Geophysical Research* 110, C10S06, doi:10.1029/2004JC002769.
- Kovacevic, V., Gacic, M., Mancero Mosquera, I., Mazzoldi, A., Marinetti, S., 2004. HF radar observations in the northern Adriatic: surface current field in front of the Venetian Lagoon surf. *Journal of Marine Systems* 51, 95–122.
- Lafite, R., Shimwell, S., Grochowski, N., Dupont, J.-P., Nash, L., Salomon, J.-C., Cabioch, L., Collins, M., Gao, S., 2000. Suspended particulate matter fluxes through the Straits of Dover, English Channel: observations and modelling. *Oceanologica Acta* 23, 687–700.
- Le Hir, P., Bassoulet, P., Erard, E., Blanchard, M., Hamon, D., Jegou, A.M., 1986. Etude régionale intégrée du Golfe Normand-Breton. Vol. 1. Ifremer Report DERO-86.27-EL.
- Malčić, V., Viezzoli, D., Cushman-Roisin, B., 2000. Tidal dynamics in the northern Adriatic Sea. *Journal of Geophysical Research* 105 (C11), 26265–26280.
- Marmorino, G.O., Shay, L.K., Haus, B.K., Handler, R.A., Graber, H.C., Horne, M.P., 1999. An EOF analysis of HF Doppler radar current measurements of the Chesapeake Bay buoyant outflow. *Continental Shelf Research* 19 (2), 271–288.
- Matthews, J., Fox, A., Prandle, D., 1993. Radar observation of an along-front jet and transverse flow convergence associated with a North Sea front. *Continental Shelf Research* 13, 109–130.
- Ménesguen, A., Gohin, F., 2006. Observation and modelling of natural retention structures in the English Channel. *Journal of Marine Systems* 63, 244–256.
- Orbi, A., Salomon, J.C., 1988. Tidal dynamics in the vicinity of the Channel Islands. *Oceanologica Acta* 11, 55–64.
- Park, M.-J., Wang, D.-P., 2000. Tidal vorticity around a coastal promontory. *Journal of Oceanography* 56, 261–273.
- Pingree, R.D., Maddock, L., 1985a. Stokes, Euler and Lagrange aspects of residual tidal transports in the English Channel and the southern bight of the North Sea. *Journal of the Marine Biological Association of the United Kingdom* 65, 969–982.
- Pingree, R.D., Maddock, L., 1985b. Rotary currents and residual circulation around banks and islands. *Deep-Sea Research* 32, 929–947.
- Pingree, R.D., Mardell, D.T., Maddock, L., 1985. Tidal mixing in the Channel Isles region derived from the results of remote sensing and measurements in the sea. *Estuarine Coastal and Shelf Science* 20, 1–18.
- Prandle, D., 1982. The vertical structure of tidal currents. *Geophysical and Astrophysical Fluid Dynamics* 22, 29–49.
- Prandle, D., 1993. Year-long measurements of flow through the Dover Strait by H.F. Radar and acoustic doppler current profiles (ADCP). *Oceanologica Acta* 16, 457–468.
- Prandle, D., Matthews, J., 1990. The dynamics of nearshore surface currents generated by tides, wind and horizontal density gradients. *Continental Shelf Research* 10, 665–681.
- Prandle, D., Losch, S.G., Player, R., 1993. Tidal flow through the Straits of Dover. *Journal of Physical Oceanography* 23 (1), 23–37.
- Ridderinkhof, H., 1997. The effect of tidal asymmetries on the net transport of sediments in the Ems-Dollard estuary. *Journal of Coastal Research* 25, 41–48.
- Salomon, J.C., Breton, M., 1991. Long-term tidal currents in the Channel. *Oceanologica Acta SP* (11), 47–53.
- Salomon, J.C., Breton, M., Guegueniat, P., 1995. A 2D long term advection–dispersion model for the Channel and southern North Sea. Part B: transit time and transfer function from Cap de La Hague. *Journal of Marine Systems* 6, 515–527.
- Sentchev, A., Korotenko, K., 2005. Dispersion processes and transport pattern in the ROFI system of the eastern English Channel derived from a particle-tracking model. *Continental Shelf Research* 25, 2294–2308.
- Sentchev, A., Yaremchuk, M., 2007. VHF radar observations of surface currents off the northern Opal coast in the eastern English Channel. *Continental Shelf Research* 27, 2449–2464.
- Sentchev, A., Yaremchuk, M., Lyard, F., 2006. Residual circulation in the English Channel as a dynamically consistent synthesis of shore-based observations and currents. *Continental Shelf Research* 26, 1884–2004.
- Shay, L.K., Martinez-Pedraja, J., Cook, T.M., Haus, B.K., Weisberg, R.H., 2007. High-frequency radar mapping of surface currents using WERA. *Journal of Atmospheric and Oceanic Technology* 24 (3), 484.
- Shay, L.K., Lentz, S., Graber, H.C., Haus, B.K., 1998. Current structure variations detected by high frequency radar and vector measuring current meters. *Journal of Atmospheric and Oceanic Technology* 15, 237–256.
- Signell, R.P., Geyer, W.R., 1991. Transient eddy formation around headlands. *Journal of Geophysical Research* 96, 2561–2575.
- Sirovich, L., Everson, R., Manin, D., 1995. Turbulence spectrum of the Earth's ozone field. *Physical Review Letters* 74, 2611–2614.
- Stacey, M.W., Pond, S., LeBlond, P.H., 1986. An analysis of the low-frequency current fluctuations in the Strait of Georgia, from June 1984 until January 1985. *Journal of Physical Oceanography* 17, 326–342.
- Visser, A.W., Souza, A.J., Hessner, K., Simpson, J.H., 1994. The effect of stratification on tidal profiles in a region of freshwater influence. *Oceanologica Acta* 17, 369–381.
- Yoshikawa, Y., Matsuno, T., Marubayashi, K., Fukudome, K., 2007. A surface velocity spiral observed with ADCP and HF radar in the Tsushima Strait. *Journal of Geophysical Research* 112, C06022, doi:10.1029/2006JC003625.
- Zimmerman, J.T.F., 1986. The tidal whirlpool: a review of horizontal dispersion by tidal and residual currents. *Netherlands Journal of Sea Research* 20, 133–154.